Journal of Energy Chemistry 34 (2019) 104–110

Contents lists available at ScienceDirect

Journal of Energy Chemistry

journal homepage: www.elsevier.com/locate/jechem

http://www.journals.elsevier.com/journal-of-energy-chemistry/

Wet-spun poly(ionic liquid)-graphene hybrid fibers for high performance all-solid-state flexible supercapacitors

Karthikeyan Gopalsamy, Qiuyan Yang, Shengying Cai, Tieqi Huang, Zhengguo Gao, Chao Gao*

MOE Key Laboratory of Macromolecular Synthesis and Functionalization, Department of Polymer Science and Engineering, Key Laboratory of Adsorption and Separation Materials and Technologies of Zhejiang Province, Zhejiang University, 38 Zheda Road, Hangzhou 310027, Zhejiang, China

ARTICLE INFO

Article history:
Received 23 August 2018
Revised 18 October 2018
Accepted 19 October 2018
Available online 23 October 2018

Keywords:
Graphene fiber
Poly (ionic liquid)
Wet spinning
Supercapacitors
Flexibility

ABSTRACT

It is crucial to develop flexible and wearable electronic devices that have attracted tremendous interest due to their merits on compactness, flexibility and high capacitive properties. Herein we report the continuously ordered macroscopic poly(ionic liquid)-graphene fibers by wet spinning method via liquid crystal assembly for supercapacitor application. The fabricated all-solid-state supercapacitors exhibited a high areal capacitance (268.2 mF cm^{-2}) and volumetric capacitance (204.6 F cm^{-3}) with an outstanding areal energy density (9.31 μWh cm^{-2}) and volumetric energy density (8.28 mWh cm^{-3}). The fiber supercapacitors demonstrated exceptional cycle life for straight electrodes of about 10,000 cycles (94.2% capacitance retention) and flexibility at different angles (0°, 45°, 90°, 180°) along with a good flexible cycling stability after 6000 cycles (92.7% capacitance retention). To date, such a novel poly (ionic liquid)-graphene fiber supercapacitors would be a new platform in real-time flexible electronics.

© 2018 Science Press and Dalian Institute of Chemical Physics, Chinese Academy of Sciences. Published by Elsevier B.V. and Science Press. All rights reserved.

1. Introduction

Flexible energy storage devices are indispensable and yet attractive in recent years as they meet the requirements for various portable energy systems [1–4]. In particular, fiber-based supercapacitors (FSCs) are highly advantageous and promising for next generation flexible, compact and wearable electronics [5–10]. Such a flexible one-dimensional (1D) electrode has been employed in fabricating actuators [11,12], batteries [13,14] and supercapacitors [15–17], associated with light weight and compactness which paves the way for designing modern energy conversion and storage devices. Graphene fibers (GFs) possess unique characteristics composed of high electrical conductivity, mechanical flexibility, light weight, low cost, and ease of functionalization when compared to conventional fibers [18,19]. Facile wet-spinning technology has been ideal to fabricate macroscopically assembled continuous GFs and films [18,20–24]. Very recently, Gao's group has demonstrated ultra-strong wet spun GFs with an improved mechanical strength (0.1–1.45 GPa), ultrahigh stiffness (282 GPa), low weight (0.1–2 g cm^{-3}) and electrical conductivity (> 104 S m^{-1}–0.8×10^6 S m^{-1}), with advanced functionalities [25]. To improve the capacitive properties of GFs, various conductive components (CNTs, metal oxides, polymers) are incorporated into the electrodes to meet the growing demand for high performance electronic devices. On contributing towards areal capacitance and volumetric capacitance with improved energy densities, significant achievements have advanced the FSCs. For instance, co-axially wet spun polyelectrolyte-wrapped graphene/CNT core-sheath fibers have been fabricated into yarn supercapacitors to offer a specific capacitance of 177 mF cm^{-2} by employing solid electrolytes with an energy density of 3.84 μWh cm^{-2} [26]. In another work, graphene/CNTs/PEDOT:PSS@CMC yarns, a three component system displayed an energy density of 13.8 μWh cm^{-2} [27]. Hollow graphene/PEDOT:PSS/VC FSCs revealed a volumetric capacitance of 143.3 F cm^{-3} reported by Qu et al. [28]. Recently, MXene/graphene fibers have demonstrated superior supercapacitive properties with average cycle life and stability [29]. However, it is still a great task to fabricate novel fiber-based electrodes with flexibility, stability, long cycle life, and durability, thereby achieving industrially feasible energy storage systems for next generation smart devices.

Alternatively, assembling polymer derivatives/graphene into macroscopic fibers with regular alignment still remains a huge challenge. Poly ionic liquid (PIL) represents a new class of functional materials comprising macromolecular-ionic liquid moieties with multi-functional properties [30], that have explored in a variety of applications, including polyelectrolytes, catalysts, sensors,

* Corresponding author.
E-mail address: chaogao@zju.edu.cn (C. Gao).

https://doi.org/10.1016/j.jechem.2018.10.007
2095-4956/© 2018 Science Press and Dalian Institute of Chemical Physics, Chinese Academy of Sciences. Published by Elsevier B.V. and Science Press. All rights reserved.

microwave absorbents and electronics [31–36]. Unlike other polymers, PIL possess multi-elements such as C, N, F, and S with self-integrated unique structure. The main advantages of PIL over other polymeric materials include chemical stability, tunable wettability, and improve the functional surface modification to offer novel electronic and ionic properties [30,36]. Also, employing PIL over IL has certain merits of spatial controllability over the IL species and durability. Owing to the distinct features, PILs have been employed as ionic conductors, actuators, dispersants, plasmonic and optical materials [30]. Such a multi-functional component within the hybrid GF system would offer great potentials in attaining high performance energy storage properties. Herein, for the first time we report facile wet spinning of PIL-GFs in ethyl acetate/dichloromethane coagulation bath. The reduced PIL-GFs (rPIL-GFs) were obtained by immersing in HI/acetic acid and the resultant rPIL-GFs were assembled for flexible all-solid-state SCs using PVA-H_3PO_4 electrolyte. In this work, a minimum quantity (1–7 wt%) of PIL was employed to prepare PIL-graphene dispersion to fabricate hybrid GFs by facile wet spinning technique. The fabricated rPIL-GF SCs exhibit excellent supercapacitive performance associated with areal specific capacitance, volumetric specific capacitance, energy density and power density. Moreover, the composite GFs demonstrated excellent cycling stability for about 10,000 cycles (94.2% capacitance retention) and flexibility at different bending angles (0°, 45°, 90°, 180°). Such a high performance PIL-GF SCs could be applied in real-time portable and wearable electronics with advantages including flexibility and compactness.

2. Experimental

2.1. Preparation of PIL, GFs, PIL-GFs and rPIL-GFs

PIL-Tf_2N was synthesized by following the previous report [37]. The chemical structure and ^1H NMR spectra of PIL-Tf_2N are presented in Fig. S1. Aqueous graphene oxide (GO) solution (20 mg/g) with lateral size ~20 μm was purchased from Hangzhou Gaoxi Technology Co. Ltd. (www.gaoxitech.com). Water in GO was replaced with DMF via repeated centrifugation and washing for three times. GFs were prepared by wet spinning of GO/DMF (2 mg/mL) in ethyl acetate/dichloro methane coagulation bath. The presence of small amount of dichloro methane (~10 mL) increased the density of coagulation bath thereby resulted in collecting the fibers with ease. PIL samples with different weight fractions (1 wt%, 3 wt %, 5 wt%, and 7 wt%) in GO/DMF were stirred for 48 h to obtain homogeneous dispersion. PIL-GFs were obtained by wet spinning of varied amount of PIL in GO/DMF dispersion in ethyl acetate/dichloro methane by following similar conditions opted for GF preparation. The reduced fibers were attained by immersing GFs and PIL-GFs in HI-acetic acid (2:3) at 90 °C for 6 h, washed with ethanol for several times and vacuum dried.

2.2. Fabrication of all-solid-state rGF SCs and rPIL-GF SCs

Two fibers (~1 cm) were placed parallel to each other at an appropriate distance (~2 mm) on a pre-cleaned PET substrate. Alternate opposite edges of fibers were fixed with copper sheet by silver glue and dried at room temperature. The fibers were coated with the PVA/H_3PO_4 gel electrolyte and vacuum-dried at room temperature to compose flexible all-solid-state FSC. SCs fabricated by rGFs and rPIL-GFs are designated as rGF SCs and rPIL-GF SCs. PVA/H_3PO_4 (1/1) gel electrolyte that also acts as a separator was prepared by stirring water (10 mL) and phosphoric acid (H_3PO_4) (10 mL) for ~30 min to obtain homogeneous solution. PVA (10 g, M_w 89,000–98,000) was then dissolved in 90 mL water at 90 °C and added to the above solution and stirred for 1 h.

2.3. Characterizations

Polarized optical microscopic (POM) characterizations were performed using a Carl–Zeiss AxioCam MRc5 microscope where the liquid samples are loaded into the capillary cells for observations. SEM images were taken on a Hitachi S4800 field-emission SEM system. X-ray photoelectron spectroscopy (XPS) measurements were performed using Thermo Scientific, ESCALAB 250Xi instrument with Al $K\alpha$ (1486.6 eV) as X-ray source at 15 kV × 12 mA (beam radius: 650 μm). Raman spectra were obtained employing an inVia-Reflex micro Raman spectroscopy system. CV, GCD and electrochemical impedance spectroscopy measurements were performed using an electrochemical workstation (CHI660E, CH Instruments Inc.). All the electrochemical tests were carried out at room temperature within the potential window extending from 0 to 1 V.

3. Results and discussion

Fig. 1(a) shows the scheme for the fabrication of wet spinning of PIL-GFs. PIL-GFs prepared from different weight fractions (1 wt%, 3 wt%, 5 wt%, and 7 wt% of PIL) were reduced by immersing in HI-acetic acid and the corresponding reduced fibers are designated as rPIL-GF1, rPIL-GF3, rPIL-GF5, and rPIL-GF7. The structural evolution of GO/DMF and PIL-GO5/DMF was observed by POM (Fig. 1b and c). For GO/DMF, the Schilieren texture of the lyotropic liquid-crystalline ensembles exists and the liquid-crystalline domains decreased for PIL-GO composite gel (dispersion to spin PIL-GF5) which could be attributed to the binding of PIL with GO. Surface SEM image of rPIL-GF5 is presented in Fig. 1(d). The wrinkled surface of the fiber is due to the graphene sheet shrinkage that occurred on drying process during wet spinning. Such wrinkled formations in the GFs can contribute to enhance the electrocatalytic properties. Energy-dispersive spectroscopy (EDS) mapping of the surface of PIL-GF5 is shown in Fig. 1(e–i), demonstrating the existence of C, O, N, F, and S elements. Moreover, the rPIL-GFs were observed to be flexible and realized by bending the fibers to various shapes and tied into a knot (Fig. 1(j), inset). N, F, and S are solely contributed by PIL structure and in addition to the surface-section, the distributions of elements clearly demonstrated the presence of PIL over the cross-section of graphene hybrid fiber (Fig. 2). The SEM-EDS images of rPIL-GF1, rPIL-GF3, and rPIL-GF7 are represented in Figs. S2, S3, and S4.

The chemical composition and binding state of the rPIL-GFs were investigated by X-ray photoelectron spectroscopy (XPS). Fig. 3(a) shows the XPS survey spectrum of rPIL-GF5 with C 1*s*, N 1*s*, F 1*s*, S 2*p* and O 1*s* peaks obtained at various binding energies of 284.5 eV, 401.0 eV, 688.1 eV, 163.8 eV, and 531.5 eV, respectively. The atomic composition of C, N, F, S, and O in rPIL-GF5 was found to be 75.98 at.%, 6.1 at.% 1.1 at.%, 0.7 at%, and 15.7 at.%, respectively. The nitrogen contents in rPIL-GF1, rPIL-GF3 and rPIL-GF7 were found to be 1.7 at.%, 3.2 at.%, and 6.8 at.%, respectively. The high resolution C 1*s* spectrum of rPIL-GF5 can be deconvoluted into five peaks corresponding to C–C, C–O, C–N, C=O and O–C=O at different binding energies of 284.2 eV, 285.4 eV, 286.1 eV, 287.3 eV, and 288.9 eV, respectively (Fig. S5a). N 1*s* spectrum of rPIL-GF5 persist with two deconvoluted peaks with binding energies of 399.1 eV and 401.4 eV for imidazolium-N and Tf_2-N, respectively (Fig. 3b) [36]. In case of F 1*s* spectrum, the area can be fitted to one peak centered at 688.1 eV attributable to semi-ionic C-F species, respectively (Fig. 3c) [38]. The high resolution S 2*p* spectrum was composed of three peaks centered at around 162.5 eV, 163.8 eV, and 167.2 eV corresponding to C–S bonds (S $2p_{3/2}$ and S $2p_{½}$) and SO_x species (Fig. 3d). The summary of elemental composition of PIL-GFs is listed in Table S1. The survey spectrum of rPIL-GF1, rPIL-GF3, and rPIL-GF7 are shown in Fig. S5(b).

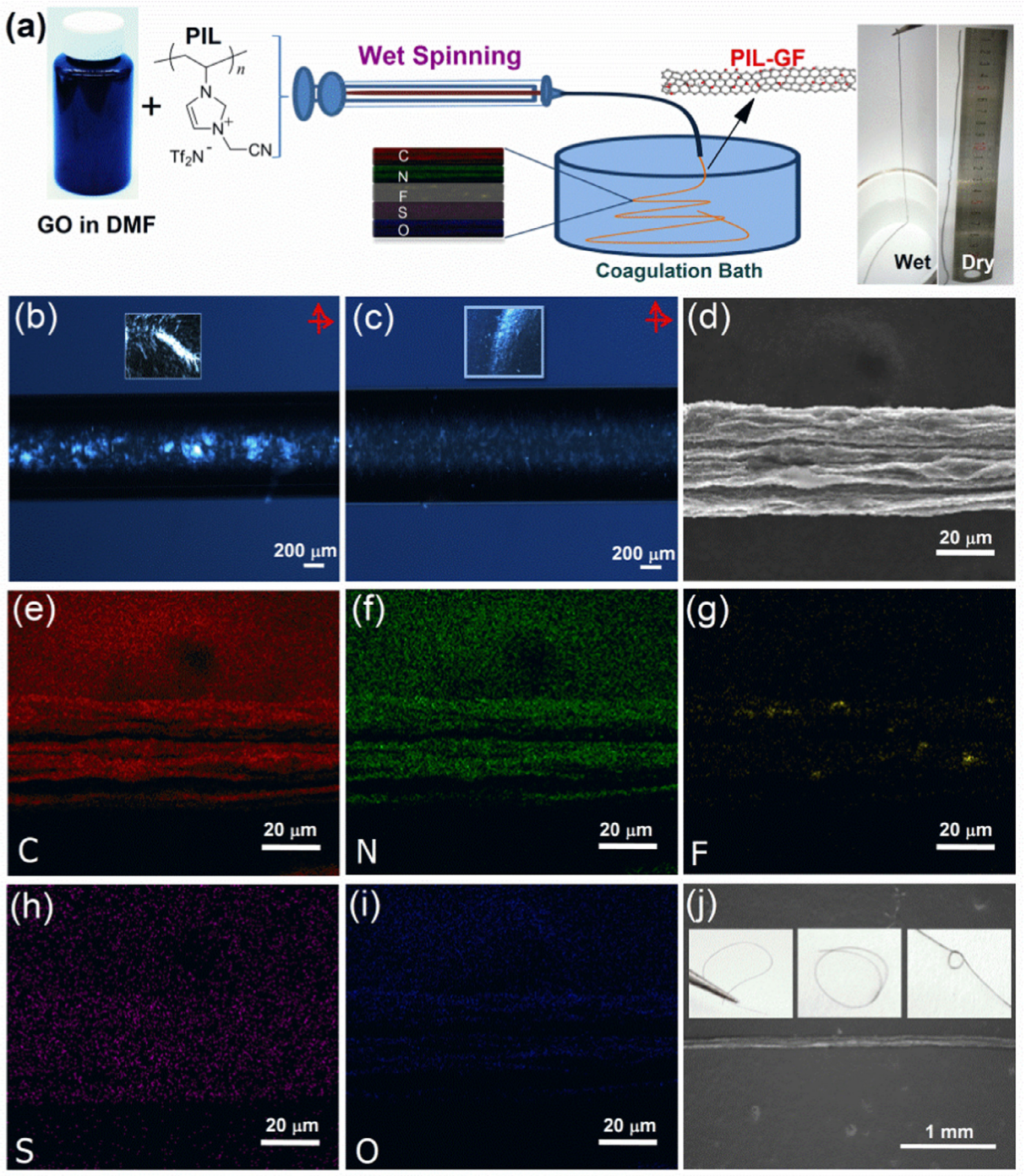

Fig. 1. (a) Schematic representation of wet spinning of continuous PIL-GFs, POM images of (b) GO/DMF and (c) PIL-GO5/DMF; (d) SEM image of surface morphology of rPIL-GF5; (e–i) elemental mapping images of rPIL-GF5 by EDS representing the distribution of C, N, F, S, and O; (j) SEM image of continuous flat rPIL-GF5; Inset in (j): photographic image of various bending shapes of rPIL-GF5.

The graphitic structure of GF and rPIL-GFs was analyzed by Raman spectroscopy (Fig. S6). Two characteristic D and G bands corresponding to carbon atoms in graphene are observed at around 1352 and 1594 cm^{-1}, which are attributed to the structural defects and first-order scattering of the E_2g mode of sp^2 carbon [39]. In general, the relative intensity ratio of D-band and G-band (I_D/I_G) in the Raman spectra is used to evaluate the amount of disorder in the graphitic materials. It was observed that the I_D/I_G ratio increases with the increase of PIL content. The calculated I_D/I_G ratio for GF was about 0.79 and the value increased from 0.81 to 1.07 for rPIL-GFs (1 to 7 wt%). The increased I_D/I_G ratio for the rPIL-GFs is attributed to the introduction of defects in the graphitic domain. Moreover, the D band peak is relatively higher than the G band peak for rPIL-GFs compared to that of GF indicating the structural modification and occurrence of supplementary defects created by the PIL bonded graphene sheets in hybrid GFs.

To evaluate the electrochemical properties of the fiber electrodes, the assembled all-solid-state FSCs with PVA/H_3PO_4 (1/1) gel electrolyte was examined using electrochemical workstation. The electrochemical performance of the fabricated FSCs was investigated by cyclic voltammetry (CV). Fig. 4(a) shows the CV curves of rPIL-GF5 at different scan rates from 10 to 100 mV s^{-1} with the

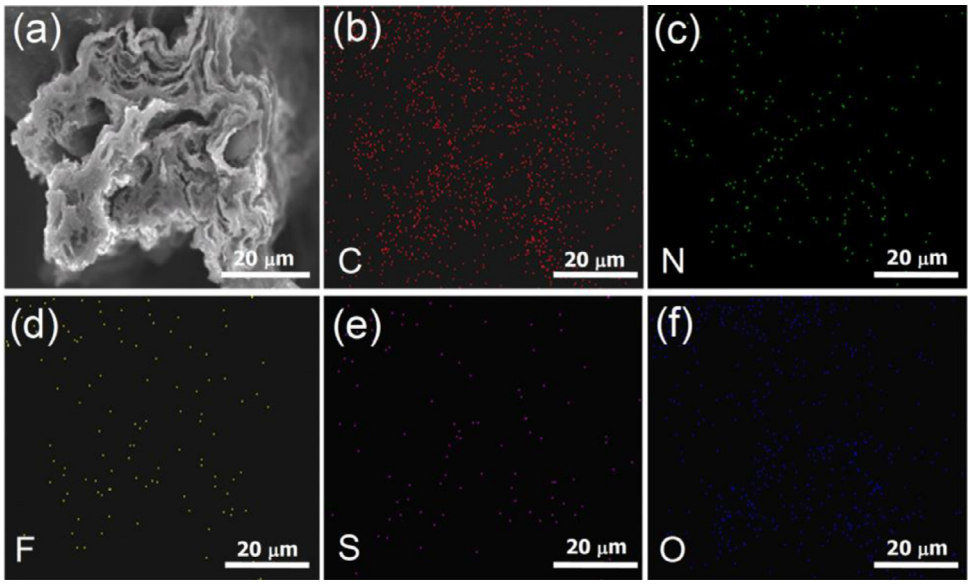

Fig. 2. (a) SEM image of cross-sectional morphology of rPIL-GF5; (b–f) elemental mapping images of rPIL-GF5 by EDS representing the distribution of C, N, F, S, and O.

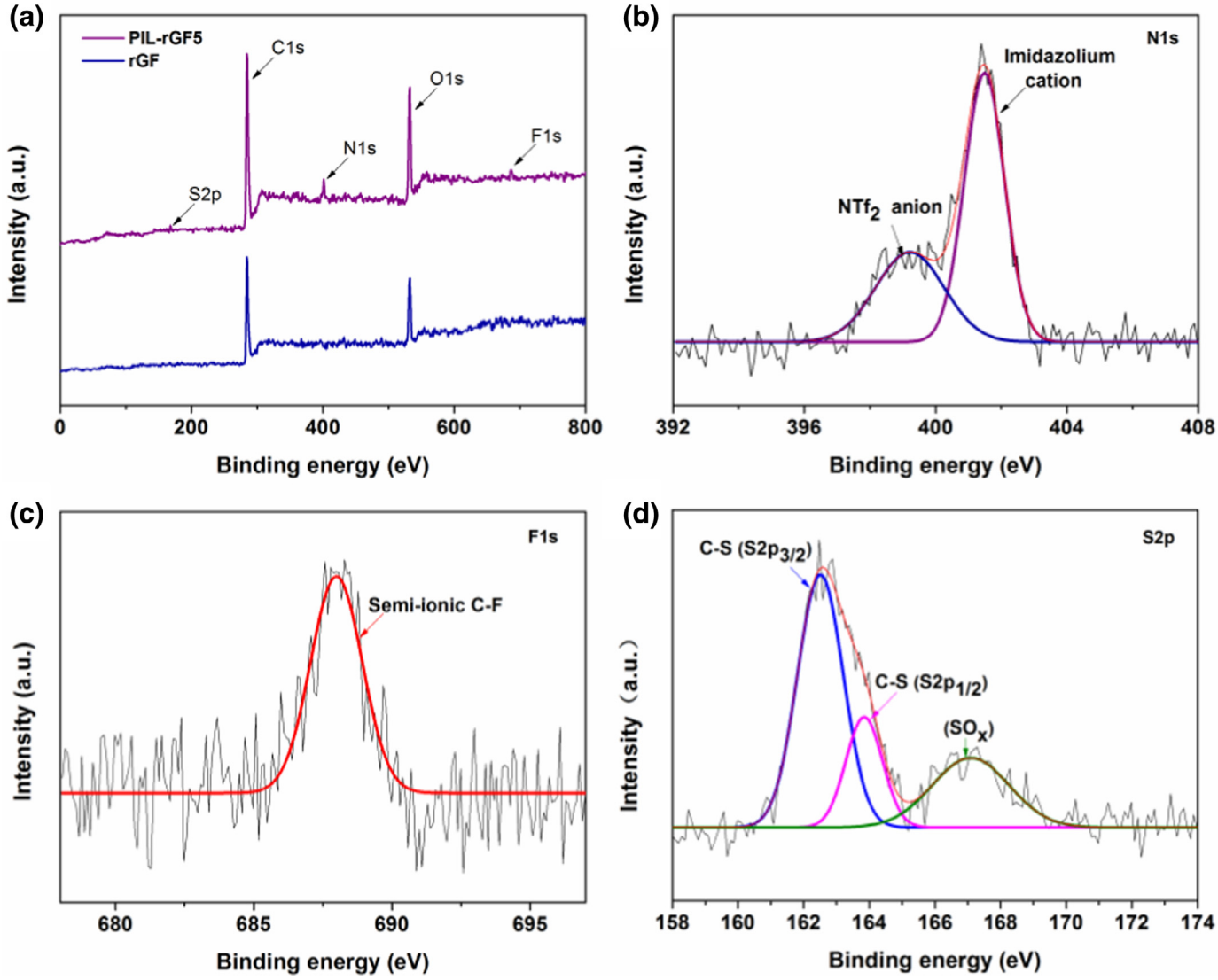

Fig. 3. (a) XPS survey spectrum of rGF and rPIL-GF5, high-resolution spectra of (b) N 1 *s*, (c) F 1 *s*, and (d) S 2*p* for rPIL-GF5.

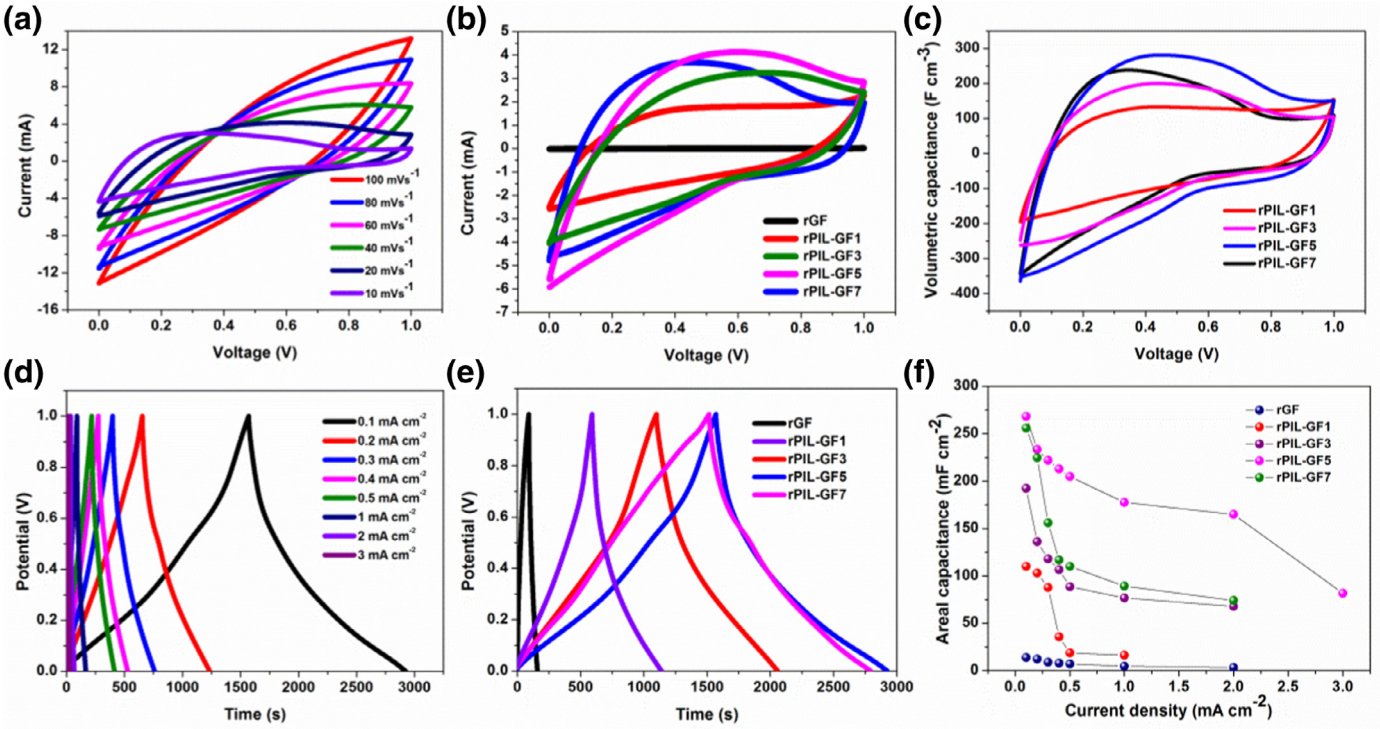

Fig. 4. (a) CV curves of rPIL-GF5 at different scan rates, (b) comparison of CV curves for various electrodes at 20 mV s^{-1}, (c) comparison of volumetric capacitances of rPIL-GF based FSCs at 10 mV s^{-1}, (d) GCD curves of rPIL-GF5 at different scan rates, (e) GCD curves of various electrodes at 0.1 mA cm^{-2}, (f) areal capacitance vs. current density plot of different FSCs.

voltage window extending from 0 to 1 V. The integral area of the PIL-GF SCs with different PIL ratios increased for 1–5 wt% and then decreased for higher PIL ratio of 7 wt%. For all the samples, the peak current increases with the increased scan rate and display a rapid current response to the voltage change, demonstrating the good electrochemical performance of the rPIL-GFs. The areal capacitance (C_A) and volumetric capacitance (C_v) were calculated from equations provided in the ESM. The capacitance increased with PIL content from rPIL-GF1 to rPIL-GF5 and decreased for rPIL-GF7 with higher PIL content. A comparison of CV curves at 20 mV s^{-1} is shown in Fig. 4(b). The highest C_A of 230.1 mF cm^{-2} and C_v of 204.6 F cm^{-3} at 10 mV s^{-1} were obtained for rPIL-GF5. C_A of rPIL-GF5 was relatively higher than those of rPIL-GF1 (102.9 mF cm^{-2} and 91.5 F cm^{-3} at 10 mV s^{-1}), rPIL-GF3 (177.5 mF cm^{-2} and 169.1 F cm^{-3} at 10 mV s^{-1}) and rPIL-GF7 (217.1 mF cm^{-2} and 184.6 F cm^{-3} at 10 mV s^{-1}). A comparison of C_v based on CV curves is shown in Fig. 4(c). The electrochemical data of the fiber electrodes are summarized in Table S2.

Galvanostatic charge-discharge (GCD) curves obtained for rPIL-GF5 at different current densities (0.1–3 mA cm^{-2}) are shown in Fig. 4(d). The summary of electrochemical data obtained for rPIL-GF5 from GCD tests is presented in Table S3. Fig. 4(e) shows the GCD curves of various electrodes at 0.1 mA cm^{-2}. The areal capacitance (C_A) obtained at different current densities for all the fiber electrodes is plotted in Fig. 4(f). The ultra-high C_A reached 268.2 mF cm^{-2} at 0.1 mA cm^{-2} (linear capacitance (C_L) = 3.86 mF cm^{-1}) for rPIL-GF5 which was far higher than that of rGF (C_A = 13.8 mF cm^{-2} at 0.1 mA cm^{-2}) by ~19 times. C_A was comparatively greater than that of previously reported CNT@PANI fibers (38 mF cm^{-2}) [40], PEDOT:PSS fibers (119 mF cm^{-2}) [41], CNT@Co_3O_4 fibers (52.6 mF cm^{-2}) [42], PANI-rGF (66.6 mF cm^{-2}) [43], PPy/rGO fiber (115 mF cm^{-2}) [44], and Bi_2O_3–NT GFs (69.3 mF cm^{-2}) [45]. A comparison of supercapacitive properties among FSCs using polymer components is presented in Table S4. The higher capacitive properties of PIL-GFs are attributed to the improved functionalities of graphene surface by the binding of PIL, surface tunability and wettability. These features offer the ease of access of electrolyte ions into the GF electrode. Additionally, the presence of N, F, and S elements within the hybrid GFs has tailored electrochemical properties that have advanced the present PIL-GF SCs. Therefore, with combining advantages, it is viable to develop such novel composite fiber electrodes to envisage superior electrochemical properties. Relatively, C_A of rPIL-GF5 was higher than that of rPIL-GF1 (110.3 mF cm^{-2} at 0.1 mA cm^{-2}–16.4 mF cm^{-2} at 1 mA cm^{-2}), rPIL-GF3 (192.4 mF cm^{-2} at 0.1 mA cm^{-2}–67.9 mF cm^{-2} at 2 mA cm^{-2}) and rPIL-GF7 (255.8 mF cm^{-2} at 0.1 mA cm^{-2}–74.21 mF cm^{-2} at 2 mA cm^{-2}). CV and GCD curves of rGF, rPIL-GF1, rPIL-GF3, and rPIL-GF7 at various current densities are presented in Figs. S7 and S8. C_A of 81.7 mF cm^{-2} was achieved for rPIL-GF5 at a high current of 3 mA cm^{-2}, respectively. C_v based on GCD curves was found to be 238 F cm^{-3}–72.7 F cm^{-3} at a current density of 0.1 mA cm^{-2}–3 mA cm^{-2}. It was observed that the electrochemical performance of rPIL-GF7 with higher PIL content was lower than that of the rPIL-GF5. This could be attributed to the aggregation of PIL and GO within the narrow limit of fiber metrics along the axis that resulted in spinning of intermittent fibers for PIL-GF7. As shown in Fig. S9(a) and (b), continuous fibers were produced till 5 wt% PIL content and at higher PIL content, for instance, the spinning dispersion of 7 wt% PIL-GO resulted in short fiber length due to the aggregation of larger particles in PIL/GO. This is evidenced by POM analysis which shows the appearance of less concentrated LCs in GO-PIL7 (Fig. S9c). The conductivity of PIL-GF5 with a diameter of 45 μm was found to be 3.7×10^3 S m^{-1}, which exhibited higher performance than those of the other fibers. The electrochemical properties of various electrodes with respective diameter and conductivity are summarized in Table S5.

To further demonstrate the stability of solid-state SC, GCD tests were carried out up to 10,000 GCD cycles for rPIL-GF5. The FSC exhibited excellent cycling stability in PVA-H_3PO_4 electrolyte,

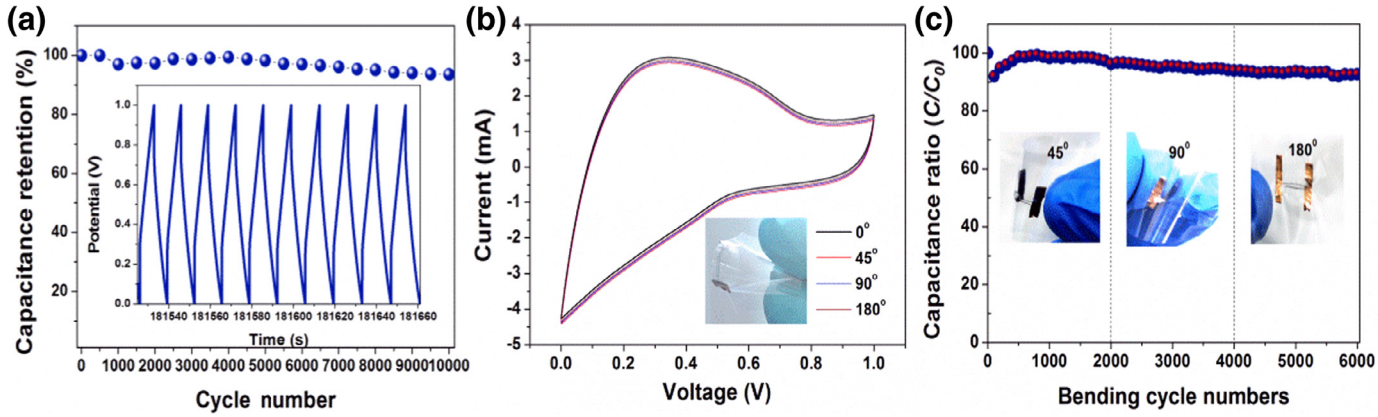

Fig. 5. (a) Cycling stability of rPIL-GF5 at 3 mA cm^{-2} for 10,000 cycles; Inset: Last 10 GCD cycles of rPIL-GF5 at 3 mA cm^{-2}. (b) CV curves obtained at 10 mV s^{-1} for different bending angles of rPIL-GF5. (c) Cycling stability of rPIL-GF5 at various bending angles.

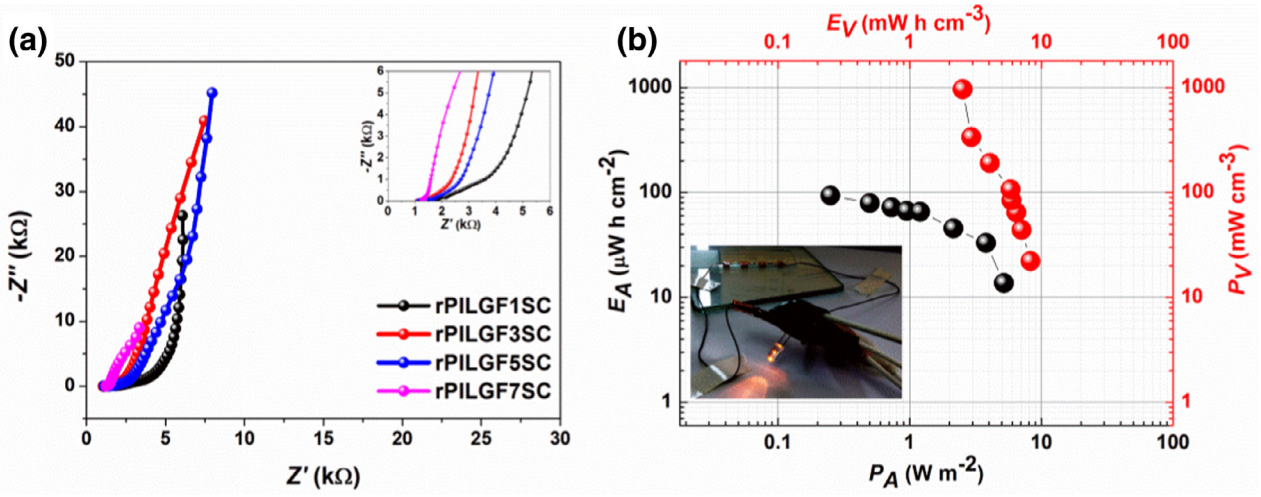

Fig. 6. (a) Niquist plot for rPIL-GFSCs, (b) Ragone plot of areal (black circles)-volumetric (red circles) energy and power densities of rPIL-GF5. Inset: Three rPIL-GF SCs connected in series power an LED.

retaining 94.2% of the initial capacitance after 10,000 GCD cycles at a high current density of 3 mA cm^{-2} (Fig. 5a). Flexibility is an imperative part in modern-electronics that has been envisaged in wearable and compact-space devices associated with multi-functional light weight electrodes (fibers or films) [46,47]. The flexibility of solid-state FSCs was investigated by evaluating the electrochemical performance under different bending angle (0°, 45°, 90°, and 180°). As shown in Fig. 5(c), no obvious change in the CV curves and capacitance values obtained at 10 mVs^{-1} for rPIL-GF5. In addition, flexible SC retained 92.7% of the initial capacitance after 6000 GCD cycles for various bending angles (45°, 90°, and 180°) (Fig. 5d). Aside from the flexibility, in order to evaluate the life time durability of the capacitor, rPIL-GF5 was analyzed at specific intervals of time, such as 3 days, two weeks and one month. A marginal decay of capacitance (~0.008 mF cm^{-2} after two weeks and ~0.003 mF cm^{-2} after one month) could be observed for long time duration (Fig. S10). Such a long durable feature could be attributed to the robustness, hybrid composite structure and compactness of solid-state rPIL-GF SCs that are advantageous to that of conventional liquid electrolyte based SCs. Nyquist plots obtained from EIS analysis of rPIL-GF SCs are shown in Fig. 6(a). The equivalent series resistances (ESR) of rPILGF1, rPIL-GF3, rPIL-G5, rPIL-GF7 SCs are 4.54 kΩ, 2.55 kΩ, 2.88 kΩ, and 1.43 kΩ, respectively. ESR is composed of three parts such as, intrinsic ohmic resistance (R_s), interfacial charge transfer resistance (R_{ct}) and warburg diffusion resistance (R_w). The Ragone plot of the rPIL-GF5 is shown in Fig. 6(b). The results revealed that the areal energy density (E_A) can reach up to 9.31 μW h cm^{-2} at 0.1 mA cm^{-2} and the high areal power density (P_A) attained about 5.1 W m^{-2} at 3 mA cm^{-2}. Moreover, the volumetric energy density (E_v) extended from 2.52 mWh cm^{-3} to 8.28 mWh cm^{-3} with volumetric power density (P_v) from 966 mW cm^{-3} to 22.2 mW cm^{-3}. Such a high supercapacitive performance of rPIL-GF electrodes could be ascribed to the hybrid composite structure of the PIL-graphene resulted from improved surface functionalities on the addition of PIL which have high binding affinity toward graphene surface. Moreover, enhanced accessibility of electrolyte ions into the hybrid rPIL-GF electrodes occurs due to the improved wettability offering superior electrochemical properties for hybrid rPIL-GF SCs. In addition, for practical application, three FSCs of rPIL-GF5 electrodes were fabricated in series to power a light emitting diode as shown in inset of Fig. 6(b).

4. Conclusions

In conclusion, the present work evidently demonstrates that multi-elemental comprised PIL-GO can be wet spun in ethyl acetate-dichloromethane coagulation bath into continuous hybrid PIL-GFs. The assembled rPIL-GFs to constitute all-solid state flexible SCs offered relatively higher areal and volumetric specific capacitances (C_A = 268.2 mF cm^{-2} and C_v = 204.6 F cm^{-3}) along with exceptional areal-volumetric energy and power densities.

Moreover, the hybrid electrodes demonstrated an excellent cycling stability after 10,000 GCD cycles, long-term durability, and flexibility at different bending angles. The hybrid PIL-GO composite structure serves the robust PIL-GFs to hold great potential as advanced electrode materials for high-performance wearable and flexible electronics.

Acknowledgments

This work is supported by the National Natural Science Foundation of China (Nos. 21325417, 51533008, and 51703194), National Key R&D Program of China (No. 2016YFA0200200), and Fundamental Research Funds for the Central Universities (Nos. 2017QNA4036 and 2017XZZX008-06).

Supplementary materials

Supplementary material associated with this article can be found, in the online version, at doi:10.1016/j.jechem.2018.10.007.

References

[1] G. Zhou, F. Li, H.M. Cheng, Energy Environ. Sci. 7 (2014) 1307–1338.
[2] W. Weng, P.N. Chen, S.S. He, X.M. Sun, H.S. Peng, Angew. Chem. Int. Ed. 55 (2016) 6140–6169.
[3] N. Liu, W. Ma, J. Tao, X. Zhang, J. Su, L. Li, C. Yang, D. Golberg, Y. Bando, Adv. Mater. 25 (2013) 4925–4931.
[4] G.H. Yu, Y. Cui, Nano Energy 2 (2013) 213–234.
[5] Y. Gogotsi, Nature 509 (2014) 568–570.
[6] W. Zeng, L. Shu, Q. Li, S. Chen, F. Wang, X.M. Tao, Adv. Mater. 26 (2014) 5310–5336.
[7] D. Yu, K. Goh, H. Wang, L. Wei, W. Jiang, Q. Zhang, L. Dai, Y. Chen, Nat. Nanotechnol. 9 (2014) 555–562.
[8] W. Jiang, S. Zhai, Q. Qian, Y. Yuan, H.E. Karahan, L. Wei, K. Goh, AndrewK. Ng, J. Wei, Y. Chen, Energy Environ. Sci. 9 (2016) 611–622.
[9] S. Zhai, C. Wang, H.E. Karahan, Y. Wang, X. Chen, X. Sui, Q. Huang, X. Liao, X. Wang, Y. Chen, Small 14 (2018) 1800582.
[10] S. Zhai, H.E. Karahan, L. Wei, Y. Wang, C. Wang, A. Montoya, Q. Shao, X. Wang, Y. Chen, Carbon 132 (2018) 698–708.
[11] Y.H. Wang, K. Bian, C.G. Hu, Z. Zhang, N. Chen, H.M. Zhang, L.T. Qu, Electrochem. Commun. 35 (2013) 49–52.
[12] H.H. Cheng, J. Liu, Y. Zhao, C.G. Hu, Z.P. Zhang, N. Chen, L. Jiang, L.T. Qu, Angew. Chem. Int. Ed. 52 (2013) 10482–10486.
[13] T. Hoshide, Y. Zheng, J. Hou, Z. Wang, Q. Li, Z. Zhao, R. Ma, T. Sasaki, F. Geng, Nano Lett. 17 (2017) 3543–3549.
[14] Y. Zhang, W. Bai, X. Cheng, J. Ren, W. Weng, P. Chen, X. Fang, Z. Zhang, H. Peng, Angew. Chem. Int. Ed. 53 (2014) 14564–14568.
[15] J. Bae, M.K. Song, Y.J. Park, J.M. Kim, M. Liu, Z.L. Wang, Angew. Chem. Int. Ed. 50 (2011) 1683–1687.
[16] Z. Yang, J. Deng, X. Chen, J. Ren, H. Peng, Angew. Chem. Int. Ed. 52 (2013) 13453–13457.
[17] F. Meng, W. Lu, Q. Li, J.H. Byun, Y. Oh, T.W. Chou, Adv. Mater. 27 (2015) 5113–5131.
[18] Z. Xu, C. Gao, Nat. Commun. 2 (2011) 571.
[19] J.C. González, E.C. Mart´ınez, M.D. Lima, M. Acik, D.M. Rogers, J. Sovich, C.S. Haines, X. Lepró, M. Kozlov, A. Zhakidov, Y. Chabal, R.H. Baughman, Adv. Mater. 42 (2012) 5695–5701.
[20] Z. Xu, C. Gao, Acc. Chem. Res. 47 (2014) 1267–1276.
[21] Z. Liu, Z. Li, Z. Xu, Z. Xia, X. Hu, L. Kou, L. Peng, Y. Wei, C. Gao, Chem. Mater. 26 (2014) 6786–6795.
[22] Y.J. Liu, Z. Xu, W.W. Gao, Z.D. Cheng, C. Gao, Adv. Mater. 29 (2017) 1606794–1606830.
[23] Z. Xu, L. Peng, Y.J. Liu, Z. Liu, H.Y. Sun, W.W. Gao, C. Gao, Chem. Mater. 29 (2017) 319–330.
[24] Z. Li, Z. Liu, H.Y. Sun, C. Gao, Chem. Rev. 115 (2015) 7046–7117.
[25] Z. Xu, Y. Liu, X. Zhao, L. Peng, H. Sun, Y. Xu, X. Ren, C. Jin, P. Xu, M. Wang, C. Gao, Adv. Mater. 28 (2016) 6449–6456.
[26] L. Kou, T. Huang, B. Zheng, Y. Han, X. Zhao, K. Gopalsamy, H. Sun, C. Gao, Nat. Commun. 5 (2014) 3754.
[27] S. Cai, T. Huang, H. Chen, M. Salman, K. Gopalsamy, C. Gao, J. Mater. Chem. A 5 (2017) 22489–22494.
[28] G. Qu, J. Cheng, X. Li, D. Yuan, P. Chen, X. Chen, B. Wang, H. Peng, Adv. Mater. 28 (2016) 3646–3652.
[29] Q. Yang, Z. Xu, B. Fang, T. Huang, S. Cai, H. Chen, Y. Liu, K. Gopalsamy, W. Gao, C. Gao, J. Mater. Chem. A 5 (2017) 22113–22119.
[30] J. Yuan, M. Antonietti, Polymer 52 (2011) 1469–1482.
[31] A. Pourjavadi, S.H. Hosseini, M. Doulabi, S.M. Fakoorpoor, F. Seidi, ACS Catal. 2 (2012) 1259–1266.
[32] Q. Zhao, M. Yin, A.P. Zhang, S. Prescher, M. Antonietti, J. Yuan, J. Am. Chem. Soc. 135 (2013) 5549–5552.
[33] J. Yuan, D. Mecerreyes, M. Antonietti, Prog. Polym. Sci. 38 (2013) 1009–1036.
[34] J. Tang, M. Radosz, Y. Shen, Macromolecules 41 (2008) 493–496.
[35] T.T. Tung, C.P. Huu, I. Janowska, T. Kim, M. Castro, J. Feller, Small 11 (2015) 3485–3493.
[36] T.Y. Kim, H.W. Lee, M. Stoller, D.R. Dreyer, C.W. Bielawski, R.S. Ruoff, K.S. Suh, ACS Nano 5 (2011) 436–442.
[37] Q. Zhao, P. Zhang, M. Antonietti, J. Yuan, J. Am. Chem. Soc. 134 (2012) 11852–11855.
[38] J. Zhang, L. Dai, Angew. Chem. Int. Ed. 55 (2016) 13296–13300.
[39] K.N. Kudin, B. Ozbas, H.C. Schniepp, R.K. Prud'Homme, I.A. Aksay, R. Car, Nano Lett. 8 (2008) 36–41.
[40] K. Wang, Q. Meng, Y. Zhang, Z. Wei, M. Miao, Adv. Mater. 25 (2013) 1494–1498.
[41] D. Yuan, B. Li, J. Cheng, Q. Guan, Z. Wang, W. Ni, C. Li, H. Liu, B. Wang, J. Mater. Chem. A 4 (2016) 11616–11624.
[42] F. Su, X. Lv, M. Miao, Small 11 (2015) 854–861.
[43] T. Huang, B. Zheng, L. Kou, K. Gopalsamy, Z. Xu, C. Gao, Y. Meng, Z. Wei, RSC Adv. 3 (2013) 23957–23962.
[44] X. Ding, Y. Zhao, C. Hu, Y. Hu, Z. Dong, N. Chen, Z. Zhang, L. Qu, J. Mater. Chem. A 2 (2014) 12355–12360.
[45] K. Gopalsamy, Z. Xu, B. Zheng, T. Huang, L. Kou, X. Zhao, C. Gao, Nanoscale 6 (2014) 8595–8600.
[46] J. Di, X. Zhang, Z. Yong, Y. Zhang, D. Li, R. Li, Q. Li, Adv. Mater. 28 (2016) 10529–10538.
[47] Q. Yang, Z. Xu, C. Gao, J. Energy Chem. 27 (2018) 6–11.